Highlights

Robust design optimisation under lack-of-knowledge uncertainty

Conradus van Mierlo, Augustin Persoons, Matthias G.R. Faes, David Moens

- A novel framework is introduced for robust design optimisation under lack-of-knowledge uncertainty
- The proposed method is demonstrated and validated on different cases, including higher dimensional problems
- A measure for the robustness is introduced based on the minimal interval width of the output quantity

Robust design optimisation under lack-of-knowledge uncertainty

Conradus van Mierlo[a,*], Augustin Persoons[a], Matthias G.R. Faes[b], David Moens[a]

[a] *KU Leuven, Department of Mechanical Engineering, Jan De Nayerlaan 5 2860, Sint-Katelijne-Waver, Belgium*
[b] *TU Dortmund University, Chair for Reliability Engineering, Leonhard-Euler-Strasse 5, 44227 Dortmund, Germany*

Abstract

Design optimization is common practice in engineering where the goal is to find the optimal combination of design parameters under prescribed constraints. However, some parameters may be impossible to define in a deterministic sense and may only be known with significant uncertainty. This limitation has led to an alternative definition of design optimality called robustness, where attention is payed to the variation around the optimal performance. Straightforward methods to solve robust optimization problems are usually limited in two ways: (1) the computation burden of the so-called 'double-loop' optimization problem hinders application to realistic models, and (2) the formalisms are typically limited to probabilistic descriptions of the uncertainty. This paper presents a formulation of the robust optimization problem under interval uncertainty and proposes a new approach taking advantage of the so-called adaptive Gaussian processes to solve it efficiently. The proposed surrogate approach mitigates the computational burden of the resolution, and a dedicated learning function is proposed to ensure iterative minimization of the surrogate modelling error and convergence towards the robust optimum. The algorithm uses a stopping criterion related to the level of confidence associated with the optimality of the solution. The approach is illustrated on six analytical and engineering benchmark problems.

Keywords: robust optimisation, interval analysis, Gaussian Process modeling, efficient global optimisation

1. Introduction

Current engineering practice involves the development and design of products that span an ever growing field of applications, while the performance of these products should also be guaranteed under a wide range of circumstances. In other words, the performance of a product should be only minimally affected by, e.g., load variations, changing environments, boundary conditions. The idea of products and processes that are insensitive to variations, e.g., in manufacturing, was pioneered by *Genichi Taguchi* who first applied his methodology on electrical circuits [1, 2]. However, the description of these variations, including the details about their underlying probability density functions (PDF's), is in general a challenging task. The main reasons for this are that the corresponding quantities are inherently variable, e.g. wind loads, there is incomplete knowledge about the quantity, e.g. direct measurement is challenging, or the designer is faced with a combination of both [3]. Additionally, in an early design stage, where the fundamental design decisions are made, only rough estimations of the quantities influencing the performance might

*Corresponding author
Email address: koen.vanmierlo[at]kuleuven.be (Conradus van Mierlo)

exists. Historically, in engineering practice uncertainties are covered by safety factors. Although this approach is very straightforward, these safety factors will not provide information about the actual conservatism in the design. Therefore, numerous techniques for uncertainty quantification have been introduced during the last decades to account for these uncertainties. Typically, these techniques are categorised as probabilistic and possibilistic approaches [4]. The latter includes techniques as: interval [5, 6], fuzzy sets [7], information gap methods [8], and imprecise probabilities [9, 10]. In general, probabilistic methods are best suited for aleatory uncertainties as they describe non-determinism via random variables defined by their joint probability distributions, while possibilistic approaches are usually well suited to cover both aleatory and epistemic uncertainties.

In addition to the variety of possibilistic methods, different definitions of the robustness are proposed in literature; the relevance of which depends on, e.g., the application and the available information. For a review of different robustness measures under probabilistic uncertainty the reader is referred to the work in [11, 12, 13]. In the context of possibilistic uncertainties, robustness definitions have been introduced in the framework of information gap theory [14, 15], convex models [16], and for fuzzy sets [17]. The definitions in these works are mainly based on two criteria: the first is minimising the variation of the output [17], and the second is to optimise simultaneously both the output (e.g. performance) and its variance around the optimal value [18, 19, 20]. In addition to the definition of robustness, a range of methods have been developed for its evaluation, with sampling strategies for most mixed uncertainty problems [17, 21], forward or inverse propagation [1], meta-model assisted methods [22], and fully decoupled methods for reliability based design optimisation [23].

This work focuses on developing a meta-model assisted method to determine the robustness at different design points. The meta-model that is used is a Gaussian Process (GP) model also known as Kriging [24, 25], which is used in this contex as an emulator of the physical model. After calibration of the GP-model on a set of evaluated points, i.e., Design of Experiments (DOE), the model is fast to evaluate. Based on this easy to evaluate GP model, fast approximations can be made about the underlying problem, i.e., numerical model, and this approximation can be improved by increasing the calibration points in the DOE. The well-known framework of Efficient Global Optimisation (EGO) [26] successfully exploits the GP mean and variance to select additional calibration points and improve on the predicted minimum. In the specific case of interval uncertainties, the GP is used to estimate the interval width in un-sampled regions, including the confidence bounds about this estimate. Hence, the GP estimate can be used in place of the actual model for the optimization problem. The estimation will be affected by a modeling error but can be bounded by a confidence interval. An improvement function is proposed that finds the next point to evaluate as a compromise between its estimated robustness and the uncertainty regarding its estimation (high GP variance). The improvement function in this paper is based on the work of M. De Munck et al. [27]. However, in this work some adaptions are proposed to the improvement function to efficiently perform the robust optimisation. To solve the robustness optimisation efficiently two improvement functions are combined: first an improvement of the interval width throughout the domain and second an improvement towards the most robust design. The combination of these two improvement functions provides a powerful improvement function that refines the GP model both globally and locally around the most robust design point. The proposed Robustness under Lack-of-Knowledge method is abbreviated as RuLoK.

This paper is structured as follows: Section 2 describes the terminology and notation that is used. In section 3 the robustness measure under interval uncertainty is introduced, while Section 4 provides the details towards the Gaussian Process model that is used. Section 5 describes the

adaptive sampling strategy that is used to calibrate the Gaussian process and the performance of this method is demonstrated on a number of cases in Section 6. Finally, in section 7 a discussion about the results is held before conclusions are drawn in Section 8.

2. Terminology and notation

In this paper, a vector is indicated as lower-case boldface characters $\mathbf{x}$, matrices are expressed as upper-case boldface characters $\mathbf{X}$ and interval parameters are indicated using apex I: x^I. Further, a distinction is made between design parameters and uncertain parameters.

Design parameters: $\mathbf{z} \in \mathcal{Z} \subseteq \mathbb{R}^{n_z}$ with $\mathcal{Z}$ the set of admissible designs and $n_z \in \mathbb{N}$, are controlled and part of the design problem, e.g., plate thickness, hole diameters.

Uncertain parameters: $\mathbf{x} \in \mathbf{x}^I \subseteq \mathbb{IR}^{n_x}$ are uncontrollable, purely epistemic parameters with $n_z \in \mathbb{N}$, typically modeled by intervals that represent, e.g., wind loads, electrical resistance, transmission parameters. The uncertain parameter vector $\mathbf{x}$ is represented as an interval vector $\mathbf{x}^I = [x_1^I, x_2^I, \ldots, x_{n_x}^I]$, with $x_i^I,\ i, \ldots, n_x$ the i^{th} parameter interval. An interval is considered *closed* when both the upper and lower bounds are a member of the interval. The domain of a real-valued interval is denoted as $\mathbb{IR}$.

3. Robustness under lack-of-knowledge uncertainty

The uncertainty considered in this work is purely epistemic in nature and results from a lack-of-knowledge about the exact value of the parameter. In practice, this kind of uncertainty is encountered when the best estimate of a parameter is limited to a range of possible values, even when its based on all available data and/or knowledge. The *real* value of the quantity, be it deterministic or variable, is in this case represented by the bounds between which it is deemed to lie. Precisely, an interval is defined as:

$$\mathbf{x}^I = [\underline{\mathbf{x}}; \overline{\mathbf{x}}] = \{\mathbf{x} \in \mathbb{R}^{n_x} \mid \underline{\mathbf{x}} \leq \mathbf{x} \leq \overline{\mathbf{x}}\}, \tag{1}$$

where $\underline{\mathbf{x}}$ denotes the lower bound and $\overline{\mathbf{x}}$ denotes the upper bound. In addition, an interval can be represented by the centre point $\hat{\mathbf{x}} = \frac{\underline{\mathbf{x}}+\overline{\mathbf{x}}}{2}$ and radius $\Delta\mathbf{x} = \frac{\overline{\mathbf{x}}-\underline{\mathbf{x}}}{2}$ of the interval.

3.1. Propagation of interval valued uncertainty

In this work the model m is a continuous function on $\mathbb{R}$, which is parameterised by a parameter vector $\boldsymbol{\theta}$. The parameter vector consists out of two parts $\boldsymbol{\theta} = \{\mathbf{x}, \mathbf{z}\}$, with $\mathbf{x}$ the uncertain parameters and $\mathbf{z}$ the design parameters. The number of elements in the parameter vector are indicated by $n_{\boldsymbol{\theta}} = n_x + n_z$. By solving the model m the parameter vector $\boldsymbol{\theta}$ is transformed $\mathbb{R}^{n_{\boldsymbol{\theta}}} \mapsto \mathbb{R}$ to a scalar response quantity $y \in \mathbb{Y} \subset \mathbb{R}$, with the set of admissible model parameters $\mathbb{Y}$, defined as:

$$m : y = m(\boldsymbol{\theta}). \tag{2}$$

The main goal of the interval analysis is to identify the extremes of the set of system responses $\tilde{y}$. Since finding the set $\tilde{y}$ is in general computationally intractable, the exact solution set is often approximated by a realisation set $\tilde{y}_s$ defined as [28]:

$$\tilde{y}_s = \left\{ y_j \mid y_j = m(\boldsymbol{\theta}_j); \mathbf{x}_j \in \mathbf{x}^I; j = 1, \ldots, n_q \right\}. \tag{3}$$

The set $\tilde{y}_s$ is typically constructed by performing n_q deterministic evaluations $y_j = m(\boldsymbol{\theta}_j)$ of the numerical model, with y_j the response of the j^{th} solution. For each of these n_q solutions, a sample is taken within the range of the interval $\mathbf{x}^I$. The main challenge herein is choosing x_j such that $\tilde{y}_s$ is a accurate approximation of $\tilde{y}$. A first way to obtain such approximation is to follow an optimisation approach. Here, the exact solution set $\tilde{y}$ is approximated by an accurate interval for the one dimensional case. For the higher dimensional case a conservative approximation is made about the hyper-cubic solution set in higher dimensions $\mathbf{y}^I = [y_1^I, y_2^I, \ldots, y_{n_y}^I]$, with $\tilde{y} \subseteq \mathbf{y}^I$. The corresponding optimisation problem is defined as:

$$\begin{aligned} \underline{y} &= \min_{\mathbf{x} \in \mathbf{x}^I} m(\boldsymbol{\theta}), \\ \overline{y} &= \max_{\mathbf{x} \in \mathbf{x}^I} m(\boldsymbol{\theta}), \end{aligned} \tag{4}$$

where $y^I = [\underline{y}; \overline{y}]$ is the solution interval. When a global minimum or maximum is found through optimisation, the exact output set bounds are obtained. However, it should be noted that the behaviour of the goal function with respect to the uncertain parameters is unpredictable in the case of strongly non-linear problems, which makes the computational effort highly problem dependent [29].

There is a special case for monotonic problems, where the vertices of the hyper-cubic input space are sampled, called the vertex method, introduced by Dong and Shah [30]. Following this method the output set is determined exactly within 2^{n_x} evaluations. However, the underlying assumption is that the model output behaves monotonically with respect to the input parameters, which is not true in general. Other approaches are intrusive methods to solve interval problems, which have been proposed in [31], and interval arithmetic methods as proposed in [32].

3.2. Defining robustness in the case of interval valued uncertainty

As mentioned in the introduction, multiple definitions of robustness exist, depending on the context and application. In this work, it is proposed to define robustness as the design with minimum variation in the performance given a well-defined input uncertainty. Following this definition, robustness can be defined as the ratio of input uncertainty to the output uncertainty. However, quantifying this uncertainty is non-trivial in general. Therefore, the focus lies on the interval radius as a measure for the uncertainty. In this way, this robustness measure can be regarded as an interval counterpart to robustness measures that minimize the variance of the performance. For a case with one interval valued input parameter, the input and output uncertainty are represented respectively by the scalar interval radius Δx and the associated scalar output interval radius Δy. The output radius is a function of the design parameter $\mathbf{z}$ and should be evaluated for multiple designs $\mathbf{z} \in \mathcal{Z}$. The robustness for this case is defined as:

$$R(\mathbf{z}) = \frac{\Delta x}{\Delta y(\mathbf{z})} = \frac{\overline{x} - \underline{x}}{\overline{y}(\mathbf{z}) - \underline{y}(\mathbf{z})}, \tag{5}$$

Since Δx is independent of the design $\mathbf{z}$, finding the most robust design $\mathbf{z}^*$ is reformulated to the minimisation of the output uncertainty, which can be evaluated for multidimensional cases, defined by:

$$\mathbf{z}^* = \operatorname*{argmin}_{\mathbf{z} \in \mathcal{Z}} [\overline{y} - \underline{y}] = \operatorname*{argmin}_{\mathbf{z} \in \mathcal{Z}} [\max_{\mathbf{x} \in \mathbf{x}^I} m(\boldsymbol{\theta}) - \min_{\mathbf{x} \in \mathbf{x}^I} m(\boldsymbol{\theta})]. \tag{6}$$

Figure 1 illustrates the proposed robustness measure R for a point $\mathbf{z}^*$ and shows the associated upper bound $\overline{y}(\mathbf{z})$ and lower bound $\underline{y}(\mathbf{z})$, in red and blue. The point $\mathbf{z}^*$ is also the point with

the maximum robustness R, indicated in orange. As suggested from Equation (6) finding the robustness of just one design involves a global optimisation to construct the conservative approximation of the solution set $\tilde{y}$, which should be repeated for each of the design points in $\mathcal{Z}$. Thus, crude optimisation of the problem described in Equation (6) involves two other optimisation problems: first an optimisation that actively looks for the upper-bound $\overline{y}$, and second, an optimisation that searches the lower bound $\underline{y}$, both for the same design $\mathbf{z}$. Therefore, crude optimisation is a time consuming effort, as this would involve a large number of evaluations of the model m under consideration. In an attempt to alleviate this problem, the next section discusses the use of a well-designed Gaussian process model $\mathcal{G}$ that could be used in place of the model m.

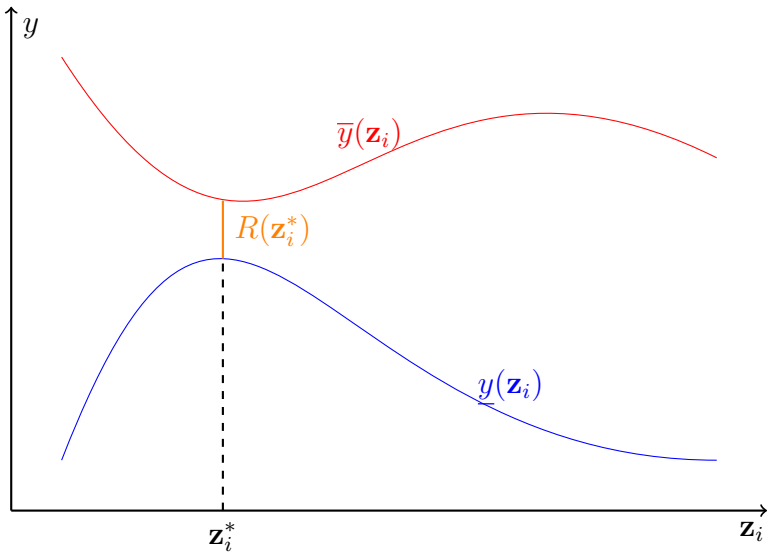

Figure 1: Illustration of the optimal robust design points $R(\mathbf{z}^*)$ (orange) for the upper and lower bounds $\overline{y}$ and $\underline{y}$ for a specific design parameter $\mathbf{z}_i$.

4. Gaussian process model for robustness under interval uncertainty

This section provides a short theoretical summary of Gaussian Process (GP) models or Kriging [24][33], an introduction with examples is also available in [34]. A GP model is a stochastic meta-model that assumes $m(\boldsymbol{\theta})$ to be a realisation of a Gaussian process, which is defined as [35]:

$$\mathcal{G} = \beta^T \mathbf{f}(\alpha) + \sigma^2 F(\mathbf{x}, \Omega), \tag{7}$$

with the first term being a deterministic regression model with $\mathbf{f}(\alpha) = \{f_1(\alpha), \ldots, f_k(\alpha)\}$ a set of arbitrary basis functions, and β^T a vector of regression coefficients. The second term consists of a zero-mean, unit variance, stationary Gaussian process $F(\mathbf{x}, \Omega)$ scaled with a constant variance of the Gaussian process σ^2. The underlying probability space of the Gaussian process is represented by Ω and the correlation between two points $\mathbf{r}$ and $\mathbf{r}'$ is defined by the covariance function $K(\mathbf{r}, \mathbf{r}', l_c)$, with l_c the characteristic length or other hyper-parameters. In general, one refers to the covariance matrix $\mathbf{K}$ where the covariance is determined for all points in a domain. The reader may refer to [36] for details about different covariance functions in Gaussian processes. In this paper two well-known covariance functions are used: The Gaussian kernel (also known as squared-exponential covariance function) and the Matérn $\frac{5}{2}$ kernel.

The GP-model is then calibrated on an initial design of experiments $\mathbf{x}_{DOE}$ obtained from, i.e., Latin hyper-cube sampling and their observed results $\mathbf{y}_{DOE}$. Conditional on the observed data the mean and the variance of the Gaussian process can be estimated [35]:

$$\mu_{gp} = \mathbf{f}(\mathbf{x})^T\hat{\beta} + \mathbf{r}(\mathbf{x})^T K^{-1}(\mathbf{y}_{DOE} - \mathbf{F}\hat{\beta}), \tag{8}$$

$$\sigma^2_{gp} = \sigma^2\left(1 - \mathbf{r}^T(\mathbf{x}) + \mathbf{u}^T(\mathbf{x})(\mathbf{F}^T\mathbf{K}^{-1}\mathbf{F})^{-1}\mathbf{u}(\mathbf{x})\right), \tag{9}$$

with $\mathbf{F}$ the matrix of the observed trend, $\mathbf{r}(\mathbf{x})$ a vector of cross-correlations between predicted points x and observed points, and with:

$$\hat{\beta} = (\mathbf{F}^T\mathbf{K}^{-1}\mathbf{F})^{-1}\mathbf{F}^T\mathbf{K}^{-1}\mathbf{y}_{DOE}, \tag{10}$$

the general least-squares estimate of β and

$$\mathbf{u}(\mathbf{x}) = \mathbf{F}^T\mathbf{K}^{-1}\mathbf{r}(\mathbf{x}) - \mathbf{f}(\mathbf{x}). \tag{11}$$

Equations (8) and (9) are referred to as the mean and variance of the GP predictor, respectively. The GP that is used in this work is an interpolating GP, which means that the prediction of the variance at an experimental point $\mathbf{x} \in \mathbf{x}_{DOE}$ tends to zero.

4.1. Predicting interval bounds with a Gaussian Process model

In this work a GP-model is used to predict the output of the model m with as input $\boldsymbol{\theta}$ the set of uncertain and design parameters. To this end, μ_{gp} is considered to be the best GP-estimate and σ_{gp} is the confidence over this estimate. For the specific application of estimating an output interval based on the GP-model the main interest goes to the maximum and the minimum response over the complete range of uncertainty. Therefore, the bounds of the response are estimated by:

$$\overline{y}_{gp}(\mathbf{z}) = \overline{\mu}_{gp}(\mathbf{z}) = \max_{\mathbf{x}\in\mathbf{x}^I} \mu_{gp}(\boldsymbol{\theta}), \tag{12}$$

$$\underline{y}_{gp}(\mathbf{z}) = \underline{\mu}_{gp}(\mathbf{z}) = \min_{\mathbf{x}\in\mathbf{x}^I} \mu_{gp}(\boldsymbol{\theta}). \tag{13}$$

A similar approach can be taken to identify the maximum and minimum of the confidence bounds:

$$\overline{\delta}_{\mu+\sigma}(\mathbf{z}) = \max_{\mathbf{x}\in\mathbf{x}^I} (\mu_{gp}(\boldsymbol{\theta}) + c\sigma_{gp}(\boldsymbol{\theta})), \tag{14}$$

$$\underline{\delta}_{\mu+\sigma}(\mathbf{z}) = \min_{\mathbf{x}\in\mathbf{x}^I} (\mu_{gp}(\boldsymbol{\theta}) + c\sigma_{gp}(\boldsymbol{\theta})), \tag{15}$$

$$\overline{\delta}_{\mu-\sigma}(\mathbf{z}) = \max_{\mathbf{x}\in\mathbf{x}^I} (\mu_{gp}(\boldsymbol{\theta}) - c\sigma_{gp}(\boldsymbol{\theta})), \tag{16}$$

$$\underline{\delta}_{\mu-\sigma}(\mathbf{z}) = \min_{\mathbf{x}\in\mathbf{x}^I} (\mu_{gp}(\boldsymbol{\theta}) - c\sigma_{gp}(\boldsymbol{\theta})), \tag{17}$$

with $c\sigma$ confidence bounds. The bounds of the response are estimated for each design point $\mathbf{z}$, based on Equations (12-17). Figure 2a illustrates a simplification of the GP-model output for a single uncertain parameter $\mathbf{x} \in \mathbf{x}^I$ and a single design variable $\mathbf{z} \in \mathcal{Z}$. The upper bound of the output interval is determined by Eq. (12), indicated by the red line, and using Eq. (13) the lower bound is found, indicated by the blue line. In addition, the bounds based on the mean plus variance $\mu_{gp} + c\sigma_{gp}$ are predicted by Equations (14) and (15), indicated by the red dotted and dashed lines. Similarly, the bounds based on the mean minus the variance $\mu_{gp} - c\sigma_{gp}$ are given by Equations (16) and (17) are indicated by the blue dotted and dashed lines. Moreover, two designs $\mathbf{z}^*_{gp}$ and $\mathbf{z}^{pot}_{gp}$ are shown, illustrating the predicted behaviour along the uncertain parameter

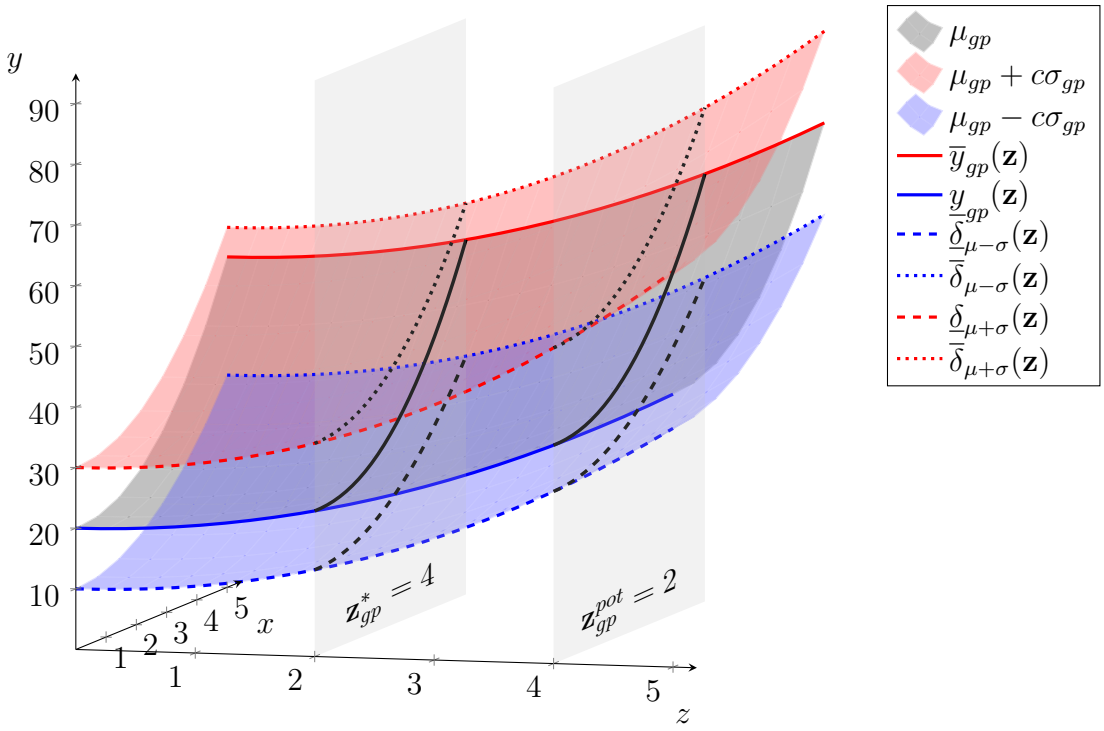

(a) Illustration of the Gaussian Prosses model spanning the uncertain $\mathbf{x}$, design $\mathbf{z}$ and output $\mathbf{y}$ space, with the GP mean prediction μ_{gp} in black and the $\mu \pm c\sigma$ CI in red and blue surfaces; Two potential design points $\mathbf{z}^*_{gp}$ and $\mathbf{z}^{pot}_{gp}$ are shown as a slice.

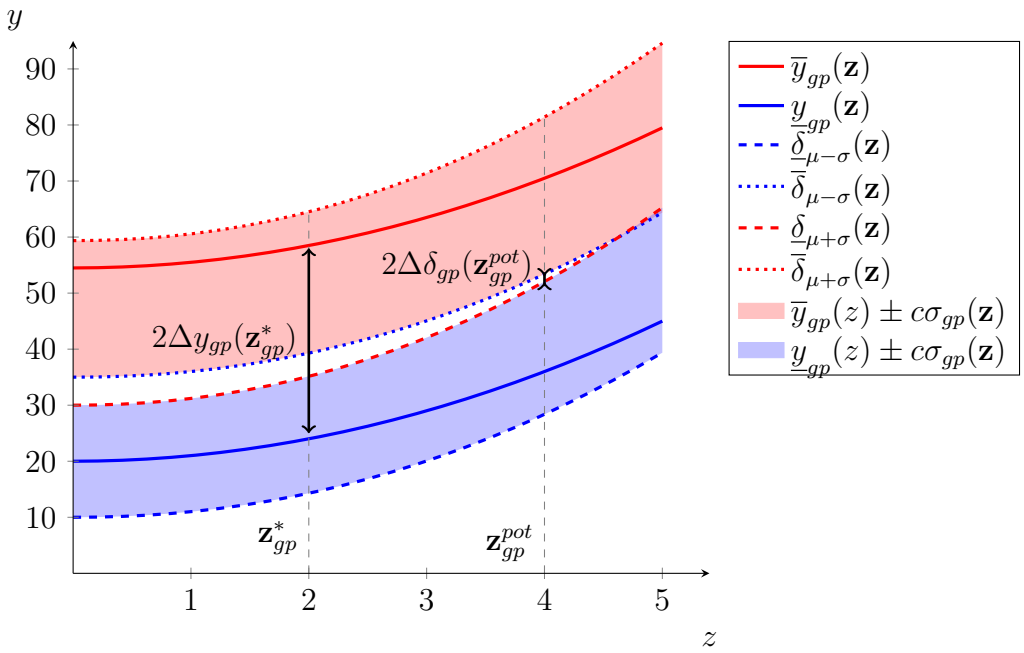

(b) Illustration of the ($\mathbf{z}$)-(y) perspective where the Confidence bounds around the upper-bound $\overline{y}_{gp}(\mathbf{z})$ and lower-bound $\underline{y}_{gp}(\mathbf{z})$ are given by the red and blue area's; and the two designs $\mathbf{z}^*_{gp}$ and $\mathbf{z}^{pot}_{gp}$ show the difference in mean bound prediction $\Delta y_{gp}(\mathbf{z}^*_{gp})$and the lowest CI prediction $\Delta\delta_{gp}(\mathbf{z}^{pot}_{gp})$ of the bounds

Figure 2: Illustration of the domain to determine the robustness based on the GP-model predictions

$\mathbf{x}$. Note that in general, for one specific design, e.g., $\mathbf{z}^*_{gp}$, the location of $\mathbf{x}$ for the predicted upper bound $\overline{y}_{gp}(\mathbf{z}^*_{gp})$ and the location of $\mathbf{x}$ of the maximum of the CI for the upper bound $\overline{\delta}_{\mu+\sigma}$ are different.

In the second illustration, Figure 2b, the estimated interval bounds are shown by the red and blue lines, with the CI about these estimates indicated by the red area for the upper bound, and blue area for the lower bound. Note that the red area is drawn between the upper bound of the minimum prediction and the upper bound of the maximum prediction by the GP-model. In addition, two designs $\mathbf{z}^*_{gp} = 2$ and $\mathbf{z}^{pot}_{gp} = 4$ are highlighted to illustrate the robustness measure. The robustness in Eq. (5) can be calculated based on these bounds given by the GP-model. Specifically, for the design $\mathbf{z}^*_{gp}$ the robustness is given by:

$$R(\mathbf{z}^*_{gp}) = \frac{\overline{x} - \underline{x}}{\overline{y}(\mathbf{z}^*_{gp}) - \underline{y}(\mathbf{z}^*_{gp})} \tag{18}$$

with $\overline{y}(\mathbf{z}^*_{gp}) - \underline{y}(\mathbf{z}^*_{gp})$ the estimated interval width, which corresponds to $2\Delta y(\mathbf{z}^*_{gp})$. Moreover, based on the CI it is also possible to estimate the potential interval width for $\mathbf{z}^{pot}_{gp}$, which would potentially have a higher robustness. To make this estimate the confidence bounds about the mean prediction are used:

$$R(\mathbf{z}^{pot}_{gp}) = \frac{\overline{x} - \underline{x}}{\overline{\delta}_{\mu-\sigma}(\mathbf{z}^{pot}_{gp}) - \underline{\delta}_{\mu+\sigma}(\mathbf{z}^{pot}_{gp})} \tag{19}$$

with $\overline{\delta}_{\mu-\sigma}(\mathbf{z}^{pot}_{gp}) - \underline{\delta}_{\mu+\sigma}(\mathbf{z}^{pot}_{gp})$ the estimated interval width, which corresponds to $2\Delta\delta_{gp}(\mathbf{z}^{pot}_{gp})$. The difference between these two robustness measures is that $R(\mathbf{z}^*_{gp})$ is estimated on the mean and the potential robustness $R(\mathbf{z}^{pot}_{gp})$ is estimated using the CI. Hence, the learning function introduced in Section 5 will exploit this difference, to search for designs with a potential higher robustness. Note that changing the constant c in Equations (14) to (17) from, e.g., 2σ to 3σ will enlarge the distance between red and blue surfaces.

In general, identifying the minimum and maximum as stated in Equations (12) until (17) is not trivial and involves numerous calls to the GP model. In addition, the mean and variance of the GP model are hard to use for optimisation as in the general case the problem is non-convex. Therefore, using a GP model is challenging for global optimisation methods. However, a number of successful strategies have been proposed to efficiently optimise such problems e.g., using branch and bound algorithms as proposed in [26]. In this work, the continuous problem is discretised over a grid with a fixed number of points. In that case, the complex problem of identifying the maximum and minimum reduces to identifying the highest value in a set of candidates. Note that this only works efficiently with a low number of parameters, as the computational burden increases exponentially $\mathcal{O}(n^d)$ with the d-dimensions of the problem for a full grid. In addition, an associated disadvantage is the finite accuracy achievable by the discretisation of the problem, with a finer discretisation causing a higher computational burden. The effects of discretisation can be mitigated in low dimensional problems by using a high number of grid points and changing the number of points to check the dependency of the solution on the discretisation.

5. Adaptive refinement of the Gaussian process model

To identify the robust design point in a limited number of evaluations of the model m the GP-model is adaptively refined with the specific goal of identifying the most robust design point. Therefore, the GP-model itself is used to identify regions of interest based on two criteria related to the famous compromise between exploration (low prediction confidence) and exploitation

(identified areas of possible optimum). The learning function to achieve this is described in this section, starting first with an introduction of the maximum improvement function.

5.1. Maximum improvement function

The learning function introduced in this paper is based on the maximum improvement function, which was introduced in [27]. Before applying this idea to the robustness problem as stated in the previous section, the general idea is briefly summarised. The goal of the learning function is to determine which sample is the best candidate to enrich the set of calibration samples for the GP. This effectively means improving the precision of the GP around the selected sample. Here this is illustrated on a general continuous function $f(\mathbf{u}) : \mathbb{R}^{n_u} \mapsto \mathbb{R}$, which is approximated by a GP-model $g(\mathbf{u})$. Using the learning function as defined in (20), a compromise is made between improving the calibration around the expected minimum using the GP mean (exploitation) and in areas of high prediction uncertainty based on the GP variance where a better minimum could be found (exploration). By iteratively enriching the calibration of the GP with the best sample improves the estimation of the minimum until a stopping criterion is eventually reached. The learning function is defined as [27]:

$$MI(\mathbf{u}) = \frac{\min(\mu_g(\mathbf{u})) - (\mu_g(\mathbf{u}) - c\sigma_g(\mathbf{u}))}{\min(\mu_g(\mathbf{u}))}, \tag{20}$$

with $\mu_g(\mathbf{u})$ the GP model prediction at $\mathbf{u}$, $\min(\mu_g(\mathbf{u}))$ the current minimum, and $c\sigma_g(\mathbf{u})$ represents the variance around the prediction of $\mathbf{u}$. Here, the variance is truncated at a certain confidence bound with c in Eq. (14). Hence, when the confidence bounds are based on, e.g., 3σ, more effort is dedicated to reducing the uncertainty about the approximation. Contrarily, lower confidence bounds, e.g., 2σ, reduce the confidence interval and favour improving approximately found maxima or minima. To identify the new candidate point $\mathbf{u}_{\text{new}}$ the maximum MI is identified over the domain $\mathbf{u} \in \mathcal{U}$ found by:

$$\mathbf{u}_{\text{new}} = \underset{\mathbf{u}\in\mathcal{U}}{\operatorname{argmax}} \left(\frac{\min(\mu_g(\mathbf{u})) - (\mu_g(\mathbf{u}) - c\sigma_g(\mathbf{u}))}{\min(\mu_g(\mathbf{u}))} \right). \tag{21}$$

Figure 3 shows the true function $f(\mathbf{u})$ in red and the GP based approximation $g(\mathbf{u})$ in black. The black dot is a point that is part of the DOE used to calibrate the GP-model. Furthermore, this figure shows how the learning function in Eq. (20) is used to evaluate the point $\mathbf{u}_{new} \in \mathcal{U}$ to determine which point should be added to the DOE. When the GP-model is re-calibrated using the newly evaluated point $\mathbf{u}_{\text{new}}$, the minimum of $f(\mathbf{u})$ is further approximated. If it is unlikely that a point $\mathbf{u}_{\text{candidate}}$ provides a minimum of $f(\mathbf{u})$ lower than the current $\min g(\mathbf{u})$, a negative improvement is obtained.

5.2. Maximum improvement of the robustness

After the introduction of the maximum improvement, the remainder of section 5 describes how this is used in this specific case of robustness. The main goal of the optimisation procedure is to identify the most robust design point in $\mathbf{z} \in \mathcal{Z}$, such that this design provides a minimum variation in the output interval for all $\mathbf{x} \in \mathbf{x}^I$. This is enabled by adapting the maximum improvement, introduced in Eq. (20), to work directly on the minimum interval width. Specifically, it is adapted to:

$$MI_z(\mathbf{z}) = \frac{\min_{\mathbf{z}\in\mathbf{z}^I} \left(\overline{y}_{gp}(\mathbf{z}) - \underline{y}_{gp}(\mathbf{z}) \right) - \left(\overline{\delta}_{\mu-\sigma}(\mathbf{z}) - \underline{\delta}_{\mu+\sigma}(\mathbf{z}) \right)}{\min_{\mathbf{z}\in\mathbf{z}^I} \left(\overline{y}_{gp}(\mathbf{z}) - \underline{y}_{gp}(\mathbf{z}) \right)}, \tag{22}$$

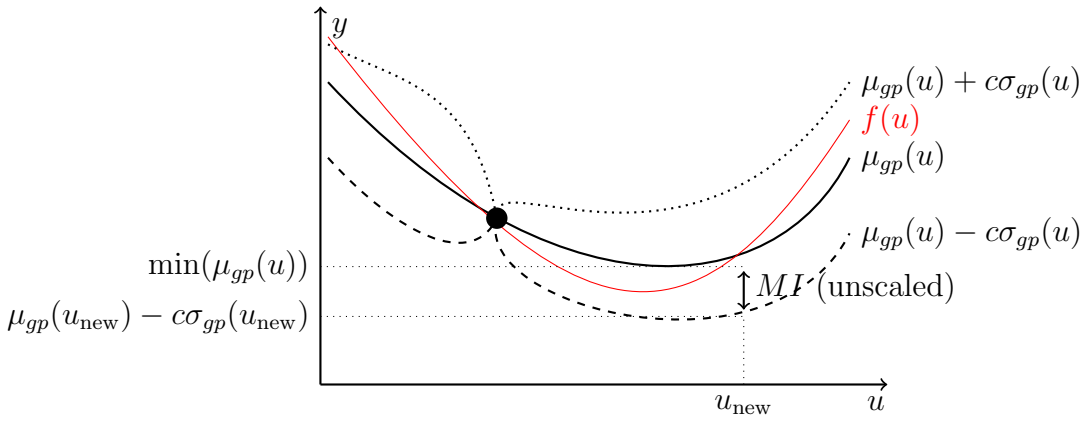

Figure 3: Illustration of the learning function where the goal is to approximate the minimum of the true function $f(u)$ in red, by the GP-model prediction $g(u)$; the black dot is point that is part of the DOE and the next point u_{new} is selected by the learning function, adapted from [27]

with $\overline{\delta}_{\mu-\sigma}(\mathbf{z}) - \underline{\delta}_{\mu+\sigma}(\mathbf{z})$ the predicted minimum bound $2\Delta\delta(\mathbf{z})$ with a confidence interval of $c\sigma$ about this bound, and $\min_{\mathbf{z}\in\mathbf{z}^I}\left(\overline{y}_{gp}(\mathbf{z}) - \underline{y}_{gp}(\mathbf{z})\right)$ the minimum bound predicted by the mean estimate. Note that the mean estimated bounds correspond to $2\Delta y_{gp}(\mathbf{z}^*_{gp})$ in Figure 2b, and $\overline{\delta}_{\mu-\sigma}(\mathbf{z}) - \underline{\delta}_{\mu+\sigma}(\mathbf{z})$ to $2\Delta\delta_{gp}(\mathbf{z}^{pot}_{gp})$ in the same figure. By reaching a $MI_z(\mathbf{z}) \leq 0$, when the two intervals are equal, one can state that it is not expected with, e.g, 95% confidence for $c = 1.96$, that there is a smaller bound of Δy within the current range of design parameters $\mathbf{z} \in \mathcal{Z}$. Figure 4 illustrates in the top graph the improvement function where $\Delta\delta$ provides a possible smaller bound for the interval Δy. In the graph below the value for $MI_z(\mathbf{z})$ is given, illustrating that it is likely to improve the robustness at $\min \Delta\delta$.

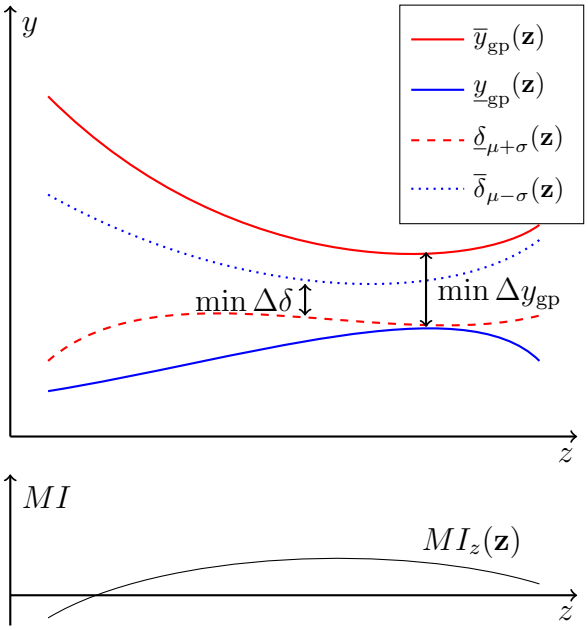

Figure 4: Illustration of the predicted mean bound $\Delta y_{\text{gp}}(\mathbf{z}) = \overline{y}_{\text{gp}}(\mathbf{z}) - \underline{y}_{\text{gp}}(\mathbf{z})$ and the minimum bound based on the confidence interval $\Delta\delta(\mathbf{z}) = \underline{\delta}_{\mu+\sigma}(\mathbf{z}) - \overline{\delta}_{\mu-\sigma}(\mathbf{z})$

5.3. Maximum improvement of the predicted bounds

The previously introduced improvement function Eq. (22) finds a promising design point, based on the estimates of the GP-model. However, to estimate promising design points the overall GP-model must be refined as well, especially around these promising design points. Therefore, a second improvement function is introduced to increase the confidence of the predicted bounds. Here the maximum improvement Eq. (20) is adapted to obtain a best estimate of the minimal interval width $\Delta\delta_{\min}$, which depends on both the upper and lower bound. Figure 5 illustrates the idea behind the improvement function used here. In general, the goal is to approximate the output set $\tilde{y}_s$ for each design $\mathbf{z} \in \mathcal{Z}$. The point that provides the largest improvement of the lower bound of this interval is given as:

$$MI_{\min}(\boldsymbol{\theta}) = \min_{\mathbf{x}\in\mathbf{x}^I} \left[\mu_{gp}(\boldsymbol{\theta}) + c\sigma_{gp}(\boldsymbol{\theta})\right] - \mu_{gp}(\boldsymbol{\theta}), \tag{23}$$

and the improvement of the upper bound is given as:

$$MI_{\max}(\boldsymbol{\theta}) = \mu_{gp}(\boldsymbol{\theta}) - \max_{\mathbf{x}\in\mathbf{x}^I} \left[\mu_{gp}(\boldsymbol{\theta}) - c\sigma_{gp}(\boldsymbol{\theta})\right]. \tag{24}$$

Note that unlike the improvement functions in Equations (20) and (22) the one given in (23) and (24) are not normalized and calculated for each design in $\mathcal{Z}$. Hence, there is a guaranteed possible improvement even if the global minimum and maximum are identified. The improvement function is illustrated in Figure 5 for a single point $\mathbf{x}^* \in \mathbf{x}^I$. In the illustrated case, the improvement of the minimum bound $MI_{\min}$ is unlikely (negative value) while it seems likely to improve the upper limit $MI_{\max}$. In the end, only one candidate point can be chosen to be added to the design of experiments. Therefore, for each evaluated point the highest improvement value is used, which can either improve the lower bound or the upper bound:

$$MI_x = \max(MI_{\min}, MI_{\max}). \tag{25}$$

This means that for the illustration in Figure 5 only the value of MI_{max} is saved for the point $\mathbf{x}^*$.

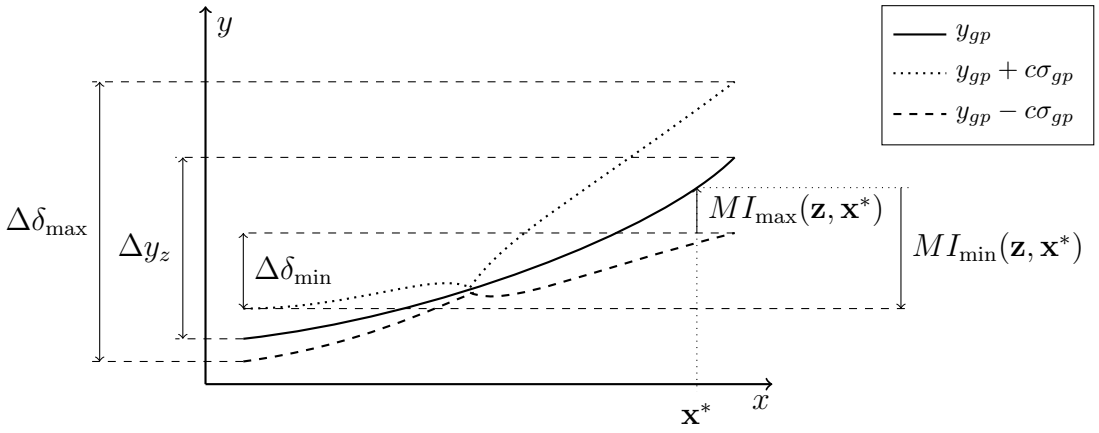

Figure 5: Illustration of the learning function for a candidate point x^*, showing the MI of the lower and upper bound; here the improvement of the lower bound is negative

Finally, the candidate point that performs best over the sum of the two improvement functions Eq. (22) and Eq. (25) is selected. Hence, the next candidate point $\boldsymbol{\theta}_{\text{candidate}}$ is obtained by:

$$\boldsymbol{\theta}_{\text{candidate}} = \underset{\mathbf{z}\in\mathcal{Z}\ \mathbf{x}\in\mathbf{x}^I}{\operatorname{argmax}} \left[MI_z(\mathbf{z}) + MI_x(\boldsymbol{\theta})\right]. \tag{26}$$

Note that it is possible here to assign weighting factors to the two functions. However, to the authors knowledge no advantage is gained in this regard. Hence, these weights are not used in this work.

5.4. Stopping criterion for adaptive refinement

The role of a stopping criterion is to indicate when the algorithm reached a desired level of convergence. In this work, the stopping criterion is defined on the improvement of the robustness MI_z, which means that based on the current GP-model it is unlikely to identify a point that is more robust than the current best estimate $\min_{\mathbf{z}\in\mathbf{z}^I}\left(\overline{y}_{gp}(\mathbf{z}) - \underline{y}_{gp}(\mathbf{z})\right)$. This point is identified with $c\sigma$ confidence when the maximum improvement $MI_z \leq 0$. However, this is only achieved when the GP-model variance at location $\mathbf{z}^*$ reduces to zero. Although possible in theory, this is highly unlikely to be achieved in practice. Hence a small error term ϵ is defined, which assures that when:

$$MI_z \leq \epsilon, \tag{27}$$

there is with 95% confidence no point R within the domain smaller than $R(1+\epsilon)$. Unless explicitly specified otherwise, the default value for $\epsilon = 1 \cdot 10^{-3}$ throughout this work.

5.5. Overview of the method

In Figure 6, a flowchart of the method is provided. The flowchart describes in detail the steps needed to perform the optimisation as proposed in this paper. The method starts at the initialisation where all parameters are selected by the user, i.e., correlation function, size of the initial design of experiments, value for ϵ. After this initialisation is made, the initial design of experiments is evaluated by the model m and the GP is calibrated. Hereafter, the adaptive refinement starts with finding new potential robust designs points based on the learning function in Section 5. For each newly identified point the model is evaluated $m(\boldsymbol{\theta}_{\text{candidate}})$ and the results are added to the Design of Experiments. This loop continues until the stopping criterion Eq. (27) is met. Finally, after finishing the optimisation, it is highly recommended to validate and verify the results of the GP. A good starting point to check the accuracy of the GP-model is to perform Leave-one-Out (LOO) cross-validation with the points already in the Design of experiments.

6. Case studies

In this section the RuLoK technique is tested and validated for different problems, which start with a set of analytical functions and build up to higher dimensional engineering examples. For the first analytical cases a comparison is made with classical optimisation techniques, which require direct evaluations of the the numerical model for each of the sample points. Moreover as the robustness measure in Eq. (6) requires a double-loop optimisation approach, where the outer-loop is focused on the next design point and the inner loop identifies the upper and lower bound of the response for a given design $\mathbf{z} \in \mathbb{Z}$. This optimisation directly uses the expensive to evaluate numerical model. Thus, the efficiency is measured in the amount of required function evaluations.

6.1. Analytical test functions

To study the basic properties of the proposed method a set of analytical test functions is used. Each of the three test functions presents a different challenge in terms of optimisation, starting form a convex and smooth function and progressing to non-convex problems. The analytical test functions are defined as:

$$f_a(x_1, x_2) = x_1^2 x_2 - x_2^2, \tag{28}$$
$$f_b(x_1, x_2) = x_2 x_1 - \sin(x_1) x_2^2 + x_1^2, \tag{29}$$
$$f_c(x_1, x_2) = \cos(4\pi x_1) - \sin(x_1 x_2) + x_2, \tag{30}$$

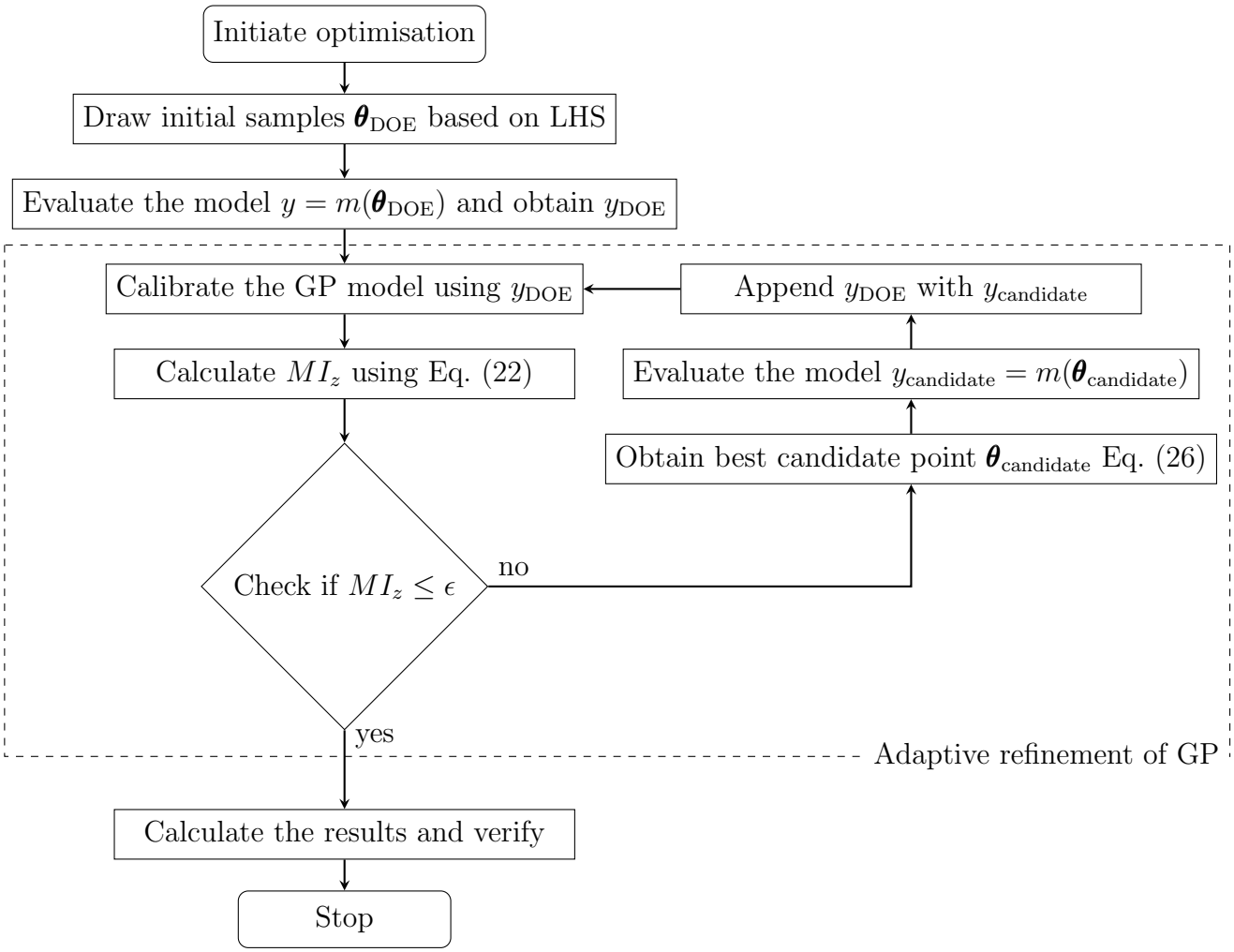

Figure 6: Flowchart of the robustness under lack-of-knowledge method

with $x_1 \in [-5, 5]$ the design parameter and $x_2^I = [-5, 5]$ the uncertain parameter. The goal of the optimisation is to identify the value for x_1 at which the bounds on Δf are minimal for each $x_2 \in x_2^I$. This optimisation is defined as:

$$\max R(x_1) = \min_{x_1 \in x_1^I} \left(\max_{x_2 \in x_2^I} f_n(x_1, x_2) - \min_{x_2 \in x_2^I} f_n(x_1, x_2) \right), \tag{31}$$

with n indicating the three functions f_a, f_b, f_c. In these particular cases, without the need for optimisation, one can determine that the minimum of the functions f_a, f_b and f_c lies at $x_1 = 0; \forall x_2 \in x_2^I$. Nevertheless to demonstrate the additional value of the proposed method two well-known optimisation algorithms are used in a comparison. These two optimisation approaches used in this work are: Unconstrained Optimisation (UO) where the minimum of a function is searched using a quasi-Newton algorithm; an other strategy is to use a Generic Algorithm (GA) to solve the outer-loop where the bounds of the response in the inner-loop are identified using UO. The population for the GA is set to a default value of 20.

The results of the method and these of the classical optimisation approaches are compared in Table 1. It is noticed that the proposed method outperforms the brute optimisation approaches, which is expected with the use of a meta-model. The table also shows that depending on the level of confidence the number of iterations increases. Note that the amount of iterations needed

to obtain a result is difficult to estimate a priori as this depends on the underlying problem and the correctness of the GP model at each iteration. The error term in the table refers to the discretization error introduced by using a fixed grid to sample the meta model. For both function f_a and f_b the optimal point is part of the samples in the grid using $n_{\text{samples}} = 501$. However, for function f_c this dependence is checked and the optimal point is not part of the grid points $n_{\text{samples}} = 200$ or $n_{\text{samples}} = 500$. Therefore, the analysis returns the next best point, which is the closest to the optimal point. Using a larger number of grid-points will therefore increase the accuracy of the estimation at a higher computational cost.

Function	Method	Optimum	Iterations	Evaluations	Error*	confidence
f_a	analytic	0	-	-	-	-
f_a	RuLoK	0	36	38	≈ 0.02	$1,96\sigma$
f_a	RuLoK	0	42	44	≈ 0.02	3σ
f_a	UO	-7e-6	3	184	-	-
f_b	analytic	0	-	-	-	-
f_b	RuLoK	0	28	30	≈ 0.02	$1,96\sigma$
f_b	RuLoK	0	49	51	≈ 0.02	3σ
f_b	GA	0.099	77	50680	-	-
f_c	analytic	0	-	-	-	-
f_c	RuLoK	-2.5e-2	279	281	0.05	$1,96\sigma$
f_c	RuLoK	1e-2	172	174	0.02	$1,96\sigma$
f_c	RuLoK	0	214	216	≈ 0.02	$1,96\sigma$
f_c	RuLoK	-1e-2	242	244	0.02	3σ
f_c	GA	4.4e-5	30	2760857	-	-

* the discretization error of the grid is determined by $\Delta x/n_{points} = 10/501$ for f_a and f_b.

Table 1: Results of the analytic test functions

To further illustrate how the method works Figure 7 shows the function value for all three functions f_a,f_b and f_c at each design point x_1. For each function the true bounds are given by the black dashed lines, the evaluated point are indicated with a green cross, and the predicted upper- and lower-bound are given in red and blue, including their 95% confidence intervals, and the optimal design point is indicated by a circle. Starting at the top of Figure 7 function f_a is shown where the gradient decreases when moving towards the robust design point $x_1 = 0$. The middle sub-figure illustrates the function f_b with larger confidence bounds around the predicted optimum, shown by the red and blue areas. It is also shown that the confidence interval about the upper bound is larger than this of the lower bound, which is exactly the goal during optimisation. Finally, the bottom graph of Figure 7 shows the more complex function f_c with the optimum at $x_1 = 0$. This figure illustrates the additional function evaluations needed to ensure the global minimum was found, and not one of the many local minimums. Note that for this case the optimal robust point $x_1 = 0$ is not part of the grid as the grid is discretized by an even number of samples, which include the end and start point.

In Figure 8 the meta-model of function f_a is plotted with the black surface the mean response, the red and blue surfaces the lower- and upper-bound of the 95% confidence intervals, and the green dots are the points used to calibrate the GP-model. This figure illustrates the dispersion of the evaluation points at the edges of the domain and concentration of points around the optimal point, which reduces the variance of the GP-model is this location. Hence, the distance between the

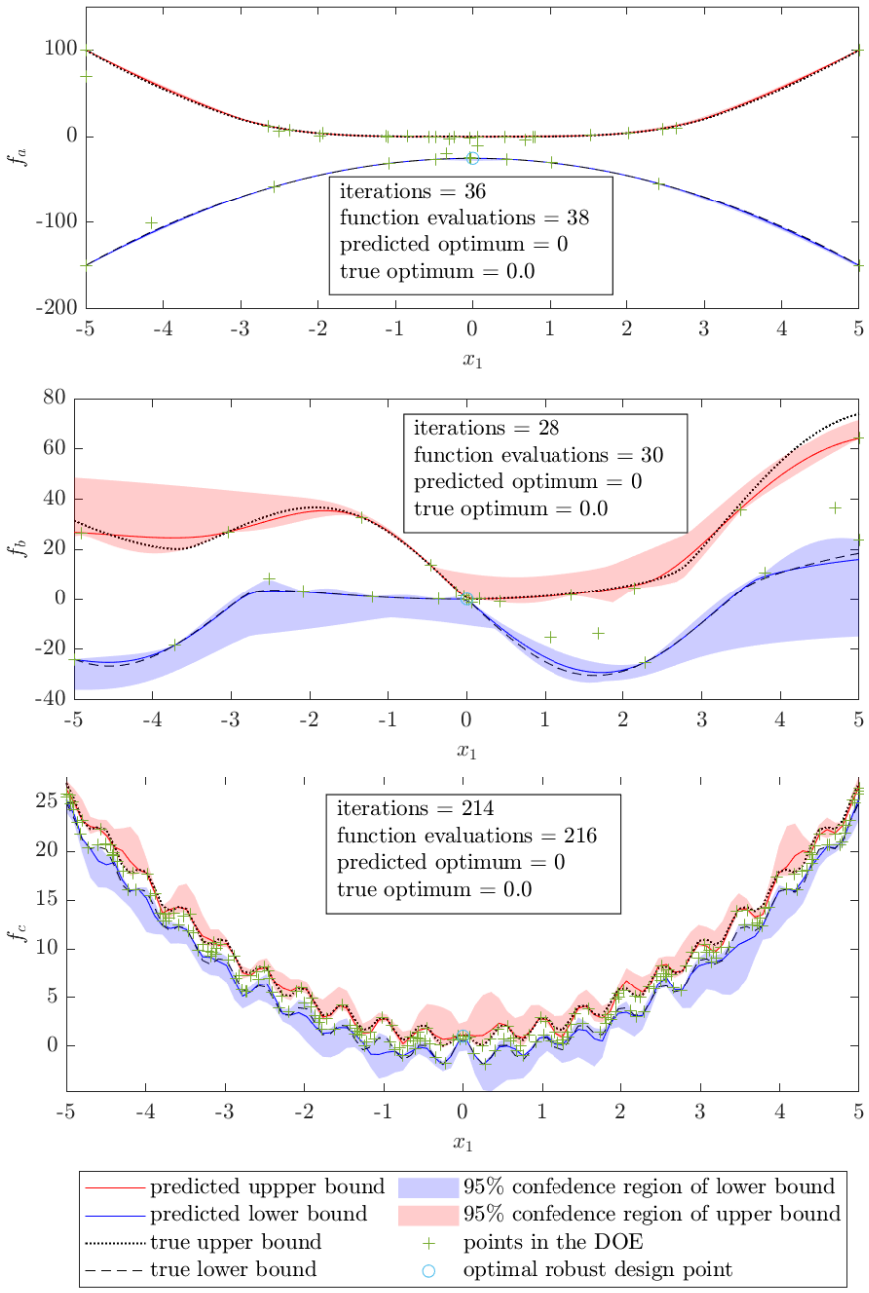

Figure 7: The GP predicted bounds of the interval valued uncertainty including the 95% confidence intervals; for from the top to the bottom function f_a,f_b and f_c, respectively.

bounds increases in locations that are further from the optimal point since there are considerably less points evaluated here. Nevertheless, it is possible to use the GP-model further to analyse the problem at hand. However, one should be aware that due to the selection of training points an overall agreement between the GP-model and the underlying problem is not guaranteed.

6.2. Plate subjected to a point load

In this case study, the thickness of a plate with two equal sides of 100mm is chosen within the interval $t \in [3,\ 6]$mm. The uncertain parameter is the Young's modulus of the material, which

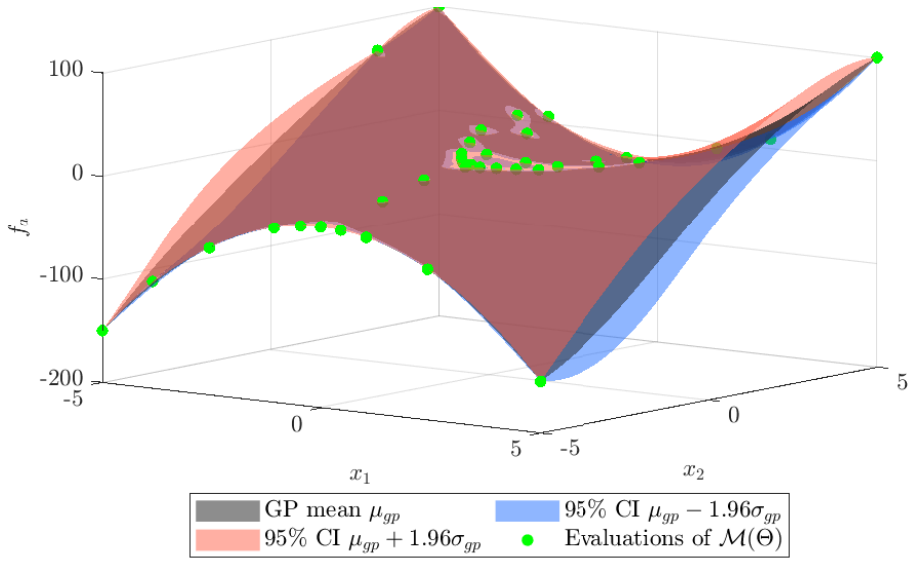

Figure 8: GP-model prediction of function A with the black surface the mean response, the red and blue surfaces the 95% CI on the mean prediction, and the green points indicating the evaluated points

is known to be bounded by the interval: $E^I = [110,\ 280]$GPa. All degrees of freedom of one side of the plate are completely fixed and a point load of 100N is applied to one of the opposite corners. The performance of this design is measured by the displacement of the corner node that is subjected to the load. The analysis is performed by a finite element model using 1000 shell elements.

At the start of the analysis two initial points are evaluated based on Latin Hyper-Cube sampling. Figure 9 shows the results that are obtained after just 9 function evaluations, with the true bounds of the model in dashed black lines, the GP-model prediction of the upper- and lower-bound in red and blue, and the confidence intervals as colored areas. The optimal design point $t_{\text{robust}} = 6$mm is as expected, the thickest plate. The rationale behind this simple example is that the thickest plate will bend less than a thinner plate under identical uncertainty of the Young's modulus. However, Figure 9 presents an illustration of the refinement around the optimal point, with only two evaluation points lower than 4.5mm. The order of the points that are added is further highlighted by the numbers next to the crosses in the plot starting with the initial evaluations 1 and 2, up to 9, the final point.

Although the physical interpretation of the problem explains the identified optimum a double-loop approach is used to validate this result. Here using CO a total of 82 evaluations of the numerical model were needed to identify the optimum $t_{\text{robust}} = 6$mm, which is identical. However, with this classical optimisation no additional information is obtained regarding the problem that is studied.

6.3. The borehole function

The second engineering example is the Borehole function [37], which is a typical test case for computer experiments. The borehole function describes the water flow f_{borehole} though a borehole between two underground aquifers by the flow rate of the water m^3/year:

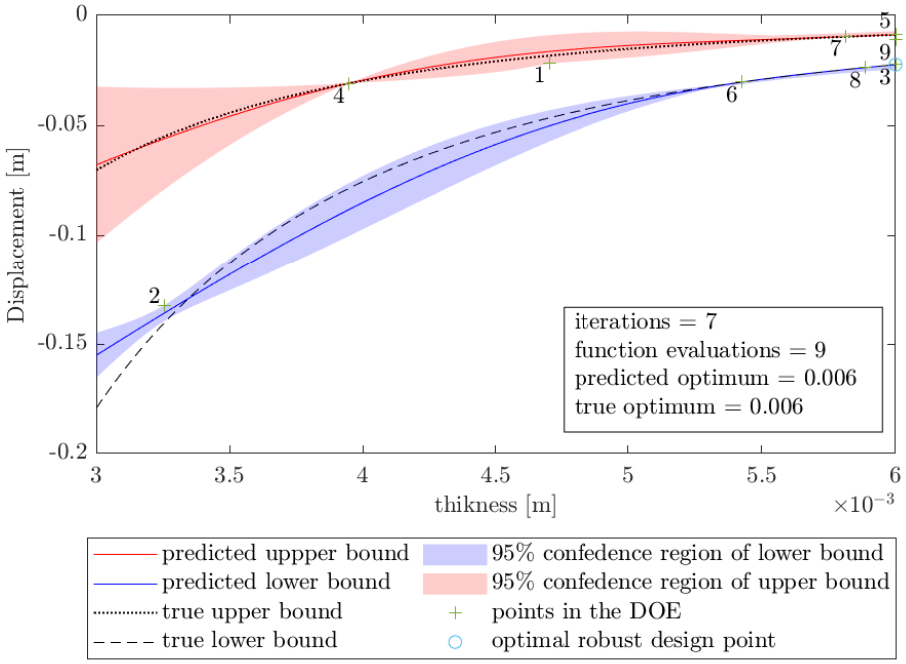

Figure 9: GP predicted bounds of the interval valued uncertainty including the order in which the points within the DOE where evaluated; including the 95% confidence intervals, evaluated points indicated by crosses, and the optimal design point indicated by a circle.

$$f_{\text{borehole}} = \frac{2\pi T_u (H_u - H_l)}{\ln\left(\frac{r}{r_w}\right)\left(1 + \frac{2LT_u}{\ln\left(\frac{r}{r_w}\right) r_w^2 K_w + \frac{T_u}{T_l}}\right)}. \tag{32}$$

It is assumed that the diameter $r_w \in [0.05, 0.15]$ m, the length of the borehole $L \in [1120, 1680]$m of the borehole can be controlled and are therefore the design parameters. All other parameters are listed in Table 2. Two cases are considered with this example, first a case where only two parameters are uncertain and the others are taken at the midpoint, second a case where all parameters are considered uncertain.

6.3.1. Borehole function with two uncertain parameters

In this first case only the potentiometric head of the upper aquifer H_u and the hydraulic conductivity K_w are regarded as uncertain. The remaining uncertain parameters are taken at the midpoint of their interval. The results of the analysis are shown in Figure 10, which shows a contour plot of the true interval width on the top, the predicted interval width based on the mean of the GP-model below, and the minimal interval width based on the 95% CI next to it. In all contour plots of Figure 10 the red circle and green dot indicate the location of the robust design point, located at the lower-bound of the diameter and the upper-limit of the length of the borehole. In addition the blue dots indicate the points where the original function was sampled. The physical interpretation of the location of the robust point is that a borehole with a smaller diameter limits the possible flow through the borehole. However, for the length of the borehole this observation is not obvious. The results in Figure 10 are obtained with a total of 35 evaluations of the borehole function including the four initial evaluations.

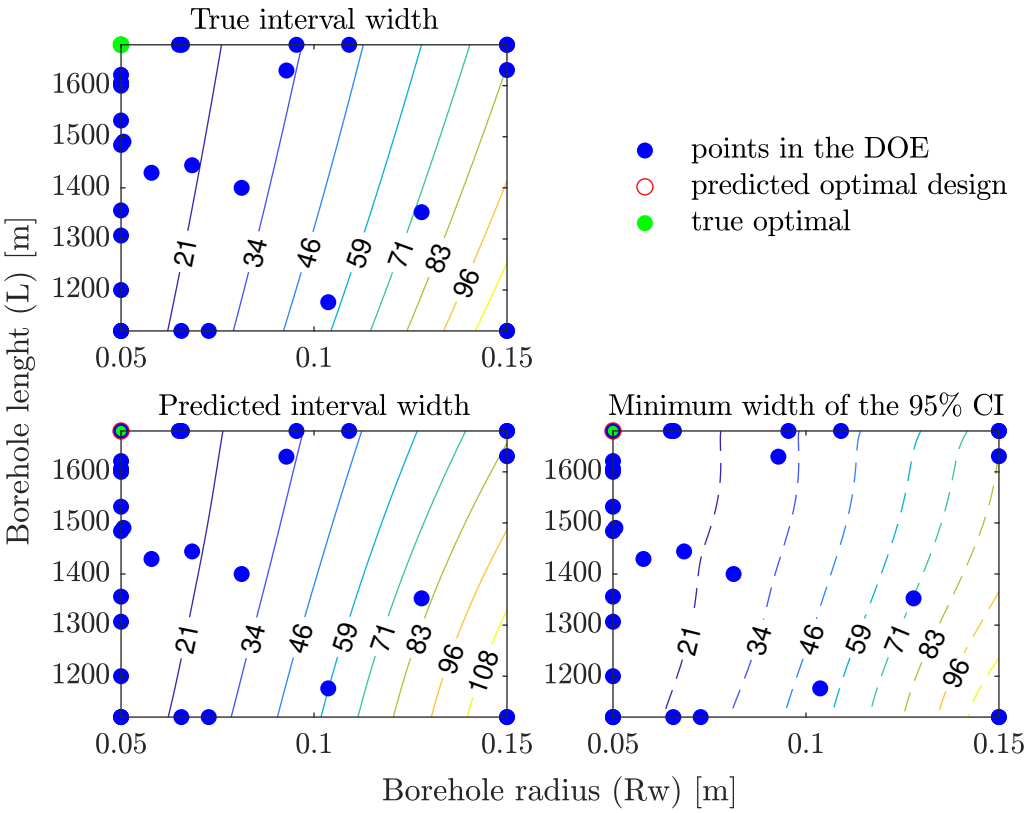

Figure 10: top: contour plot of the true interval width in function of the design parameters, borehole radius r_w and the borehole length L and only the potentiometric head of the upper aquifer H_u and hydraulic conductivity K_w are regarded uncertain; bottom: mean GP prediction of the interval width (left) and the minimal interval width by 95% CI (right)

parameter		$\underline{x}$	$\overline{x}$	$\hat{x}$	unit
radius of influence	r^I	100	50 000	2550	m
transmissivity of upper aquifer	T_u^I	63 070	50 000	56 535	m^2/year
potentiometric head of the upper aquifer	H_u^I	990	1110	1050	m
transmissivity of lower aquifer	T_l^I	63.1	116	89.55	m^2/year
the potentiometric head of the lower aquifer	H_l^I	700	820	760	m
hydraulic conductivity of the borehole	K_w^I	9855	12 045	10 950	m^2/year

Table 2: Parameters of the borehole function

6.3.2. Borehole function with six uncertain parameters

In this case all six uncertain- and the two design-parameters of the previously discussed borehole function Eq. (32) are considered within the ranges as defined in Table 2. The results of the analysis are shown in Figure 11, which shows the true interval width on the top and the GP prediction on the bottom left and the interval width based on the 95% CI on the right. The number of evaluations to obtain these results has only increased slightly to 64, which includes 8 initial evaluations, while the complexity of the problem is increased by four additional uncertain parameters. The location of the robust design point remained at the lower-bound of the diameter and the upper-bound of the borehole length. The physical reason for this difference is not directly clear from the formulation of the borehole function. However, the additional parameters seem

to have little effect to the overall behaviour of the function while the width of the interval has increased slightly, which can be seen by comparing Figure 10 and Figure 11. To better understand the effect of the additional parameters the interval sensitivities are investigated. The reader is referred to [38] for a thorough discussion about interval sensitivities. However, note that the fundamental difference between the classical sensitivity studies and interval sensitivities is that the latter is valid over the full range of the interval, while the former focuses on local sensitivities, which are not valid over the full range of the interval. The interval sensitivities for the borehole function with six uncertain parameters are provided in Figure 12, which shows that the radius of influence r, transmissivity of the upper aquifer T_u, and lower aquifer T_l have an negligible effect on the output interval. Moreover, this figure shown that all parameters behave the least sensitive around the robust design point. The latter means that with a relative change of input interval width only a minimal change in output interval width happens.

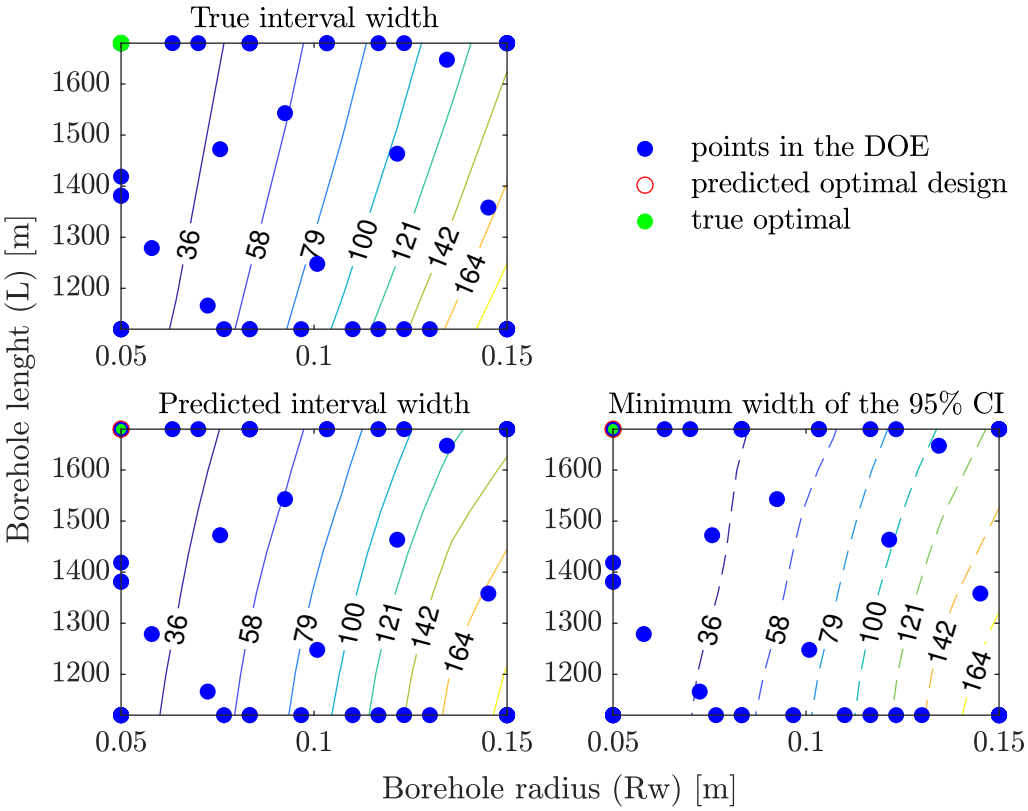

Figure 11: top: contour plot of the true interval width in function of the design parameters: borehole radius r_w, and the borehole length L; with uncertain parameters: the radius of influence r, transmissivity of upper aquifer T_u, the potentiometric head of the upper aquifer H_u, transmissivity of lower aquifer T_l, the potentiometric head of the lower aquifer H_l, the hydraulic conductivity of the borehole K_w; bottom: mean GP prediction of the interval width (left) and the minimal interval width by 95% CI (right)

Although the obtained results are convincing and could be compared with the true solution, this is not always possible especially with the use of complex numerical models. However, one can validate the GP-model based on the points that were evaluated in the Design-of-Experiments, which provides an indication about the *correctness* to capture the underlying physical behaviour. This validation is accomplished by a number of tests shown in Figure 13 which are based on the Leave-One-Out prediction of the points within the DOE. Note that this is a conservative choice

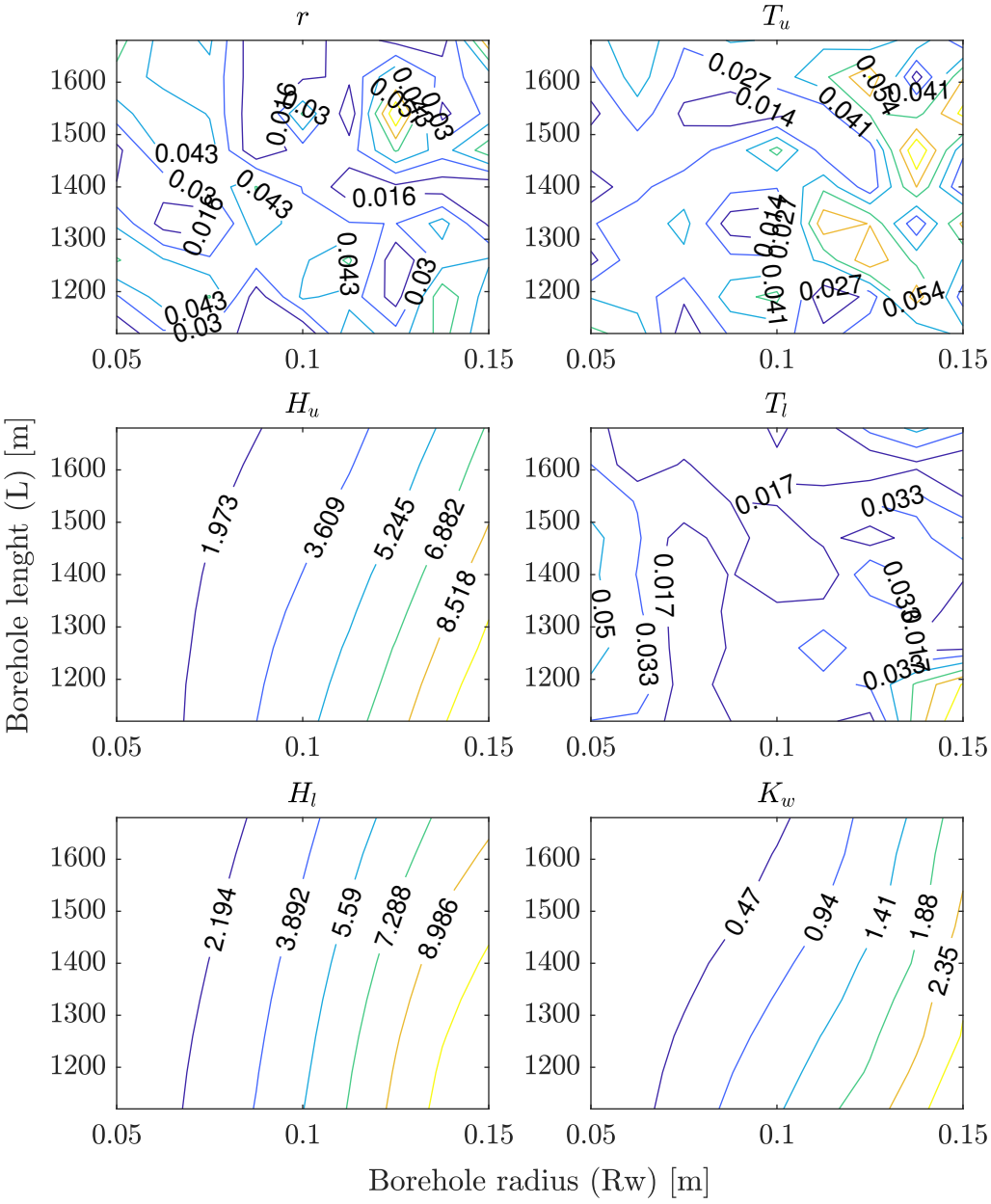

Figure 12: Relative interval sensitivity of the uncertain parameters r, T_u, H_u, T_l, H_l and K_w in function of the borehole diameter r_w and length L.

as the prediction is now made with a GP containing $n-1$ training points, which is especially conservative with a low number of training points. In Figure 13a the true function response and the Leave-One-Out (LOO) response are shown including the r^2 value. Figure 13 illustrates that most of the points in the DOE are located at the lower-bound of the function output and an increasing error towards the upper-bound of the output. The latter is a direct effect of the selection of points that are added to the DOE, which results in a GP model that is especially good in a specific region. The second Figure 13b the true function value and the standardized LOO residual are shown with the two red lines indicating the 95% CI. A similar conclusion can be made where the model in correct at lower output values but misses the true function at higher output predictions. Finally in Figure 13c the true model quantiles versus the predicted quantiles are shown. We can conclude that the GP-model performs well at low flow rates, with an error that increases at higher flow rates.

7. Discussion

In general the results of the presented method are convincing and show that this method is capable of identifying the robust design point with only a limit amount of evaluations of the underlying expensive function, which is demonstrated in a number of case studies. Nevertheless, a few things are noted by the authors that should be addressed for further research and implementation. As mentioned before, the obtained results are based on the GP model as implemented in UQlab [39] for all case studies. It is noted by the authors that using different implementations of the GP can lead to an increase in the number of iterations before convergence is reached. This is attributed to the use of a noise parameter in the GP, which is set at a minimum of $1e-4$ for the Matlab build-in implementation [40]. Hence, the error term ϵ in Equation 27 should increase to reflect this.

The number of samples in the initial DOE can effect the convergence and in this paper, as a rule of thumb, the number of initial evaluations is kept at the total amount of uncertain- and design-parameters. Quantifying the effect of the initial population size on the rate on convergence is challenging as this depends on the underlying problem, i.e., that what is resembled by the GP model. This rule of thumb is regarded as the minimal amount of initial evaluations needed by the GP to make a first estimation. Nevertheless, the number of iterations is difficult to determine a priory, as this depends on the complexity of the response surface, the added value of the point added at each iteration, and the calibration error of the GP model.

Finally, as the improvement function is evaluated on a fixed number of equally spaced grid points, a limited precision is reached. Although using a large number of grid points the precision increased, the computational cost to evaluate all these points increases exponential in d-dimensions $\mathcal{O}(n^{-d})$ for a full grid. Hence, in high dimensional cases this becomes a bottleneck without sacrificing the resolution of the grid.

8. Conclusion

This paper introduces a novel method to design robust structures in an early stage of development under lack-of-knowledge uncertainty. The presented method uses an adaptively refined GP-model to perform the global optimisation of the robustness and locate the most promising designs, which are the least sensitive to the modelled sources of uncertainty. Based on a set of analytical test functions the effectiveness and efficiency of the proposed method is demonstrated and compared with typical well-known optimisation algorithms. It is shown that the proposed

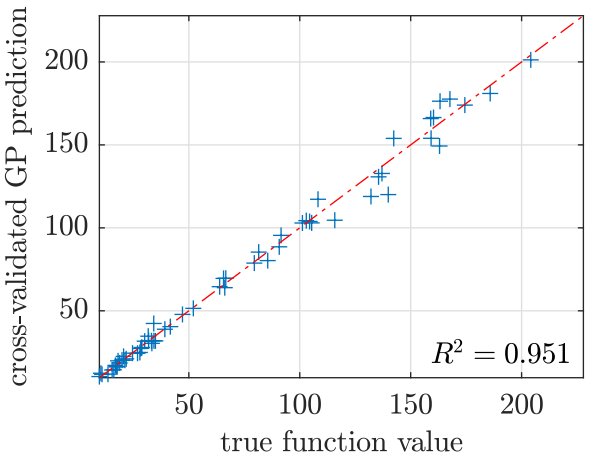

(a)

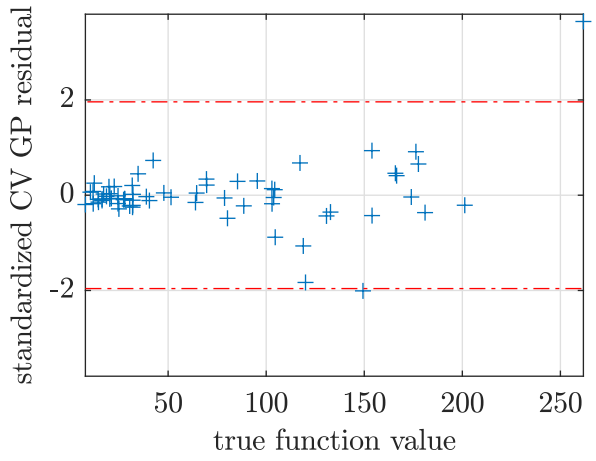

(b)

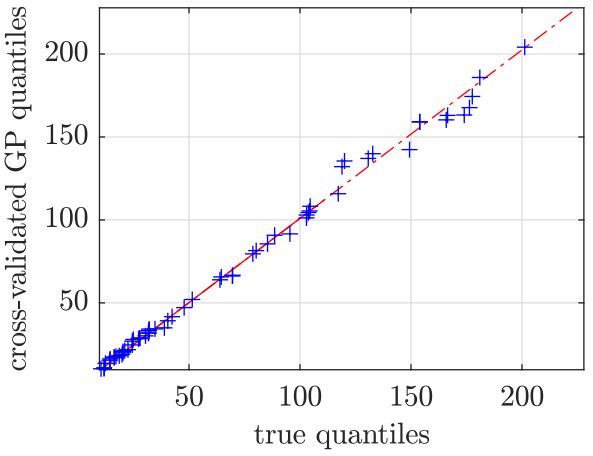

(c)

Figure 13: Validation tests for the borehole function with two uncertain parameters: (a) shows the cross-validated prediction vs. the true function value, (b) shows the standard normalized residuals of the cross-validated GP model within the 95% bounds in red, and (c) shows the cross validated quantiles vs. the true quantiles

method efficiently solves the double-loop problem, which is typically associated with robustness-based optimization methods. In addition, three additional case studies: a plate in bending, and two times the borehole function are included to demonstrate the applicability to both industrial problems and problems in moderately high dimensions. For all of these examples the results are obtained with a reasonable number of evaluations of the underlying function or numerical model. Future research is aimed at enlarging the application domain of the proposed method, specifically for time-dependant problems.

Acknowledgements

The authors gratefully acknowledge the support of the Research Foundation Flanders (FWO) under grant 1SA3919N (C. van Mierlo) and GOC2218N (A. Persoons).

References

[1] G. Taguchi, Quality engineering (taguchi methods) for the development of electronic circuit technology, IEEE transactions on reliability 44 (2) (1995) 225–229.

[2] G. Taguchi, Performance analysis design, International journal of production research 16 (6) (1978) 521–530.

[3] S. Ferson, L. R. Ginzburg, Different methods are needed to propagate ignorance and variability, Reliability Engineering and System Safety 54 (2-3) (1996) 133–144. doi:10.1016/S0951-8320(96)00071-3.

[4] G. Stefanou, The stochastic finite element method: Past, present and future, Computer Methods in Applied Mechanics and Engineering 198 (9-12) (2009) 1031–1051. doi:10.1016/j.cma.2008.11.007.

[5] M. Faes, M. Broggi, E. Patelli, Y. Govers, J. Mottershead, M. Beer, D. Moens, A multivariate interval approach for inverse uncertainty quantification with limited experimental data, Mechanical Systems and Signal Processing 118 (2019) 534 – 548.

[6] R. E. Moore, Interval analysis, Vol. 4, Prentice-Hall Englewood Cliffs, 1966.

[7] M. Hanss, Applied fuzzy arithmetic, Springer, 2005.

[8] Y. Ben-Haim, Info-gap decision theory: decisions under severe uncertainty, Elsevier, 2006.

[9] M. G. Faes, M. Daub, S. Marelli, E. Patelli, M. Beer, Engineering analysis with probability boxes: a review on computational methods, Structural Safety 93 (2021) 102092.

[10] M. Beer, S. Ferson, V. Kreinovich, Imprecise probabilities in engineering analyses, Mechanical systems and signal processing 37 (1-2) (2013) 4–29.

[11] S. Moritz Göhler, T. Eifler, T. J. Howard, Robustness Metrics: Consolidating the Multiple Approaches to Quantify Robustness, Journal of Mechanical Design 138 (11) (09 2016).

[12] M. Q. Zhang, M. Beer, C. G. Koh, H. A. Jensen, Nuanced robustness analysis with limited information, ASCE-ASME Journal of Risk and Uncertainty in Engineering Systems, Part A: Civil Engineering 2 (3) (2016) B4015001.

[13] G.-J. Park, T.-H. Lee, K. H. Lee, K.-H. Hwang, Robust design: an overview, AIAA journal 44 (1) (2006) 181–191.

[14] A. Kuczkowiak, S. Cogan, M. Ouisse, E. Foltête, M. Corus, Experimental Validation of an Info-Gap Uncertainty Model for a Robustness Analysis of Structural Responses, ASCE-ASME J Risk and Uncert in Engrg Sys Part B Mech Engrg 6 (3) (05 2020). doi:10.1115/1.4047096.

[15] T. Roach, Z. Kapelan, R. Ledbetter, M. Ledbetter, Comparison of robust optimization and info-gap methods for water resource management under deep uncertainty, American Society of Civil Engineers, 2016.

[16] F. Au, Y. Cheng, L. Tham, G. Zeng, Robust design of structures using convex models, Computers & structures 81 (28-29) (2003) 2611–2619.

[17] M. Beer, M. Liebscher, Designing robust structures–a nonlinear simulation based approach, Computers & Structures 86 (10) (2008) 1102–1122.

[18] C. Zang, M. Friswell, J. Mottershead, A review of robust optimal design and its application in dynamics, Computers & structures 83 (4-5) (2005) 315–326.

[19] N. Hu, B. Duan, An efficient robust optimization method with random and interval uncertainties, Structural and Multidisciplinary Optimization 58 (1) (2018) 229–243.

[20] I. P. Mitseas, I. Kougioumtzoglou, M. Beer, E. Patelli, J. Mottershead, Robust design optimization of structural systems under evolutionary stochastic seismic excitation, 2014, pp. 215–224. doi:10.1061/9780784413609.022.

[21] D.-S. Lee, L. F. Gonzalez, J. Periaux, K. Srinivas, Robust design optimisation using multi-objective evolutionary algorithms, Computers & Fluids 37 (5) (2008) 565–583.

[22] S. ur Rehman, M. Langelaar, F. van Keulen, Efficient kriging-based robust optimization of unconstrained problems, Journal of Computational Science 5 (6) (2014) 872–881.

[23] M. G. Faes, M. A. Valdebenito, Fully decoupled reliability-based design optimization of structural systems subject to uncertain loads, Computer Methods in Applied Mechanics and Engineering 371 (2020) 113313.

[24] D. G. Krige, A statistical approach to some basic mine valuation problems on the witwatersrand, Journal of the Southern African Institute of Mining and Metallurgy 52 (6) (1951) 119–139.

[25] J. Sacks, W. J. Welch, T. J. Mitchell, H. P. Wynn, Design and analysis of computer experiments, Statistical science 4 (4) (1989) 409–423.

[26] D. R. Jones, M. Schonlau, W. J. Welch, Efficient global optimization of expensive black-box functions, Journal of Global optimization 13 (4) (1998) 455–492.

[27] M. De Munck, D. Moens, W. Desmet, D. Vandepitte, An efficient response surface based optimisation method for non-deterministic harmonic and transient dynamic analysis, Computer Modeling in Engineering & Sciences 47 (2) (2009) 119–166.

[28] M. Faes, D. Moens, Recent trends in the modeling and quantification of non-probabilistic uncertainty, Archives of Computational Methods in Engineering 27 (2019) 633–671.

[29] D. Moens, M. Hanss, Non-probabilistic finite element analysis for parametric uncertainty treatment in applied mechanics: Recent advances, Finite Elements in Analysis & Design 47 (1) (2011) 4–16.

[30] W. Dong, H. C. Shah, Vertex method for computing functions of fuzzy variables, Fuzzy sets and Systems 24 (1) (1987) 65–78.

[31] G. Muscolino, A. Sofi, Stochastic analysis of structures with uncertain-but-bounded parameters via improved interval analysis, Probabilistic Engineering Mechanics 28 (2012) 152–163.

[32] A. Sofi, E. Romeo, A novel interval finite element method based on the improved interval analysis, Computer Methods in Applied Mechanics and Engineering 311 (2016) 671–697.

[33] C. Lataniotis, D. Wicaksono, S. Marelli, B. Sudret, UQLab user manual – Kriging (Gaussian process modeling), Tech. rep., Chair of Risk, Safety and Uncertainty Quantification, ETH Zurich,Switzerland, report# UQLab-V1.4-105 (2021).

[34] C. E. Rasmussen, Gaussian processes in machine learning, in: Summer school on machine learning, Springer, 2003, pp. 63–71.

[35] T. J. Santner, B. J. Williams, W. I. Notz, B. J. Williams, The design and analysis of computer experiments, Vol. 1, Springer, 2003.

[36] M. A. Alvarez, L. Rosasco, N. D. Lawrence, Kernels for vector-valued functions: A review, arXiv preprint arXiv:1106.6251 (2011).

[37] S. Surjanovic, D. Bingham, Virtual library of simulation experiments: Test functions and datasets, Retrieved August 19, 2021, from `http://www.sfu.ca/ ssurjano`.

[38] D. Moens, D. Vandepitte, Interval sensitivity theory and its application to frequency response envelope analysis of uncertain structures, Computer methods in applied mechanics and engineering 196 (21-24) (2007) 2486–2496.

[39] S. Marelli, B. Sudret, UQLab: A Framework for Uncertainty Quantification in Matlab, pp. 2554–2563. arXiv:https://ascelibrary.org/doi/pdf/10.1061/9780784413609.257, doi:10.1061/9780784413609.257.
URL `https://ascelibrary.org/doi/abs/10.1061/9780784413609.257`

[40] Matlab and statistics and machine learning toolbox release 2020b.
URL `https://nl.mathworks.com/help/stats/fitrgp.html`